JOURNAL OF HARD TISSUE BIOLOGY
ISSN / eISSN 1341-7649
Publisher JOURNAL HARD TISSUE BIOLOGY,
JAPANESE RED CROSS SOCIETY, 3- 24- 20, NISHIAZABU,
MINATO KU,JAPAN, TOKYO, 106-0031
Volume 26-Issue 1-(2026)
https://doi.org/10.65613/677077

Mechanism Study of the Active Ingredients in Yizhi Qingxin Formula Regulating Mitochondrial Dysfunction to Improve Alzheimer's Disease

Xiaochen Guo[1a], Lichang Yang[2b], Ziqi Ning[1c], Yaoyao Zhang[1d], Meixia Liu[1e*], Yun Wei[1f*]

1.Xiyuan Hospital, China Academy of Chinese Medical Sciences, Beijing 100091, China

2.Graduate School, Nanjing University of Chinese Medicine, Nanjing 210023, Jiangsu, China

** These authors contributed equally as corresponding authors.

aEmail: gmx80211@163.com

e*Email: meixialiu2004@126.com

Abstract

Background: Mitochondrial dysfunction is a key pathological trigger in the early stages of Alzheimer's disease (AD). Yizhi Qingxin Formula (YQF) improves mitochondrial dysfunction by regulating the PKA/CaN pathway to combat AD. However, the molecular mechanisms by which the active components of YQF treat AD remain unclear.

Aim of the study: To investigate the interaction between the active components of YQF and proteins associated with the PKA/CaN pathway, and to validate the molecular mechanism by which its active components improve mitochondrial dysfunction in AD through in vitro experiments.

Materials and methods: APP-PS1 double-gene transfected cells were set as the Model group, 293T cells as the Control group, and drug intervention groups were established based on the molecular docking results. APP-PS1 cells were intervened with the optimal drug concentration for 48 hours. The ultrastructure of cell mitochondria was observed using transmission electron microscopy (TEM); mitochondrial morphology was observed using PK Mito Orange staining; intracellular ATP concentration was determined using an ATP detection kit; mitochondrial membrane potential was detected using a TMRE detection kit; intracellular Ca^{2+} concentration was detected using the Fura Red AM Ca^{2+} probe; intramitochondrial Ca^{2+} concentration was detected using the Rhod-2 AM probe; and the expression of intracellular pathway target proteins and mRNA was detected using Western blot and Real-Time PCR.

Results: Molecular docking results indicated that Ginsenoside Rg1, Ginsenoside Rb1, Ginsenoside Re, Coptisine, Berberine, Ferulic acid, and Ligustilide exhibited strong binding affinity with the target proteins CaN, CaM, MCU, and Drp1. The active components of YQF effectively improved mitochondrial morphology in APP-PS1 cells; ameliorated mitochondrial dysfunction by increasing ATP concentration and mitochondrial membrane potential in APP-PS1 cells ($P < 0.05$); simultaneously reduced excessively high calcium ion concentrations in both APP-PS1 cells and mitochondria ($P < 0.05$); and inhibited the expression of CaN, CaM, MCU, and Drp1 proteins and mRNA in APP-PS1 cells ($P < 0.05$).

Conclusion: The active components of YQF regulate intracellular Ca^{2+} homeostasis and mitochondrial dynamic equilibrium in APP-PS1 cells by downregulating the expression of CaN, CaM, MCU, and Drp1 proteins and their respective mRNAs, thereby improving mitochondrial function. This provides theoretical support for the therapeutic potential of individual components of YQF in the treatment of Alzheimer's disease.

Keywords: Alzheimer's disease; Molecular docking; Calcium ion homeostasis; Mitochondrial dysfunction; Yizhi Qingxin Formula

1 Introduction

Alzheimer's disease (AD) is a progressive neurological condition that gradually deteriorates. The main

clinical manifestations of this condition are reduced social functioning, behavioral and psychological symptoms of dementia, and cognitive decline [1]. AD accounts for 60%-80% of dementia cases, representing the predominant form of dementia [2]. Global epidemiological data indicate approximately 50 million AD patients worldwide in 2018, with projections exceeding 100 million by 2050 [3]. China's AD patient population has approached 10 million, exhibiting a pronounced age-dependent increase in prevalence—doubling roughly every five years—imposing a heavy burden on families and society [4]. Current clinical treatments primarily rely on two classes of drugs: cholinesterase inhibitors and N-methyl-D-aspartate (NMDA) receptor antagonists. However, existing therapeutic approaches only achieve symptom relief and cannot reverse the pathological process of neuronal degeneration [5]. Against this backdrop, unraveling the mechanisms underlying AD and developing novel therapeutic agents have become critical breakthroughs for addressing the health challenges of an aging society.

The pathological mechanisms of AD exhibit multidimensional complexity, characterized by Aβ accumulation and tau protein neuronal tangles, accompanied by alterations in mitochondrial morphology and function [6]. Recent studies on AD pathogenesis have focused on inflammation, synaptic damage, oxidative stress, and mitochondrial autophagy [7,8]. Traditional Chinese medicine may improve AD by reducing Aβ deposition or neuroinflammation, modulating tau hyperphosphorylation, lowering oxidative stress levels, and regulating mitochondrial autophagy [9]. Mitochondrial dysfunction precedes Aβ deposition and serves as an initial trigger for AD [6]. Mitochondrial calcium homeostasis disruption and abnormal fission/fusion are hallmark manifestations of mitochondrial dysfunction, further accelerating AD progression [10]. An excess of Ca2+ activates dynamin-related protein 1 (Drp1), which causes a decrease in fusion and an increase in mitochondrial fission.

The research team's previous series of studies have confirmed the efficacy of the Yizhi Qingxin Formula (YQF) in treating AD models [11,12]. By regulating the protein kinase A (PKA)/calcineurin (CaN) signaling pathway, which also alters mitochondrial Ca^{2+} homeostasis and kinetic balance and diminishes mitochondrial dysfunction, it enhances learning and memory in AD mice and reduces hippocampus-related neuronal damage. This indicates that the YQF possesses therapeutic efficacy for AD, warranting further investigation into the mechanisms of action of its active ingredients [13]. Ginsenoside Rg1, Ginsenoside Re, Ginsenoside Rb1, Coptisine, Berberine, Ferulic acid, and Ligustilide were the main active ingredients of YQF, according to earlier research conducted by our team [12]. Therefore, to further investigate the binding between YQF's active ingredients and proteins related to the PKA/CaN pathway, this study employed molecular docking to screen for components with favorable docking profiles and protein targets. Cells transfected with the APP-PS1 double gene were designated as the Model group. The CCK8 assay was used to determine the optimal concentrations for each drug component, establishing the Donepezil group and YQF's individual active ingredients as drug intervention groups. Western blot, real-time PCR, Ca^{2+} fluorescent probes, and morphological analysis were employed to investigate the molecular mechanisms by which YQF's active ingredients improve mitochondrial dysfunction in AD. This study provides theoretical support for the clinical application of single-component Chinese herbal medicines in treating AD.

2 Materials and Methods

2.1 Cell Line

The 293T cell line and APP-PS1 stably transfected cell line were purchased from Shanghai Yubo Biotechnology Co., Ltd. and cultured in a 37°C, 5% CO_2 incubator.

2.2 Medications

Donepezil Hydrochloride (MCE Inc., Catalog No. HY-B0034); Ginsenoside Rg1 (Chengdu Herbpurify Co., Ltd., Catalog No. 22427-39-0), Ginsenoside Rb1 (Chengdu Herbpurify Co., Ltd., Cat. No. 41753-43-9), Ginsenoside Re (Chengdu Herbpurify Co., Ltd., Cat. No. 52286-59-6), Coptisine (Chengdu Herbpurify Co., Ltd., Cat. No. 3486-66-6); Berberine (Chengdu Herbpurify Co., Ltd., Cat. No. 2086-83-1); Ferulic acid (Chengdu Herbpurify Co., Ltd., Cat. No. 1135-24-6); Ligustilide (Chengdu Herbpurify Co., Ltd., Catalog No. 4431-01-0).

2.3 Reagents

DMEM High Glucose Medium (Gibco, USA, Cat. No. C11995500BT), Fetal Bovine Serum (Gibco, USA, Cat. No. 10099141C), Penicillin-Streptomycin Dual Antibiotics (Gibco, USA, Cat. No. 15140122); Cell Counting Kit-8 (CCK8) Cell Proliferation and Cytotoxicity Assay Kit (Dojindo, Japan, CK04); Fura Red AM Calcium Ion Fluorescent Probe (Solaibao Technology Co., Ltd., Beijing, Catalog No. IF2800); Rhod-2 AM Calcium Ion Concentration Detection Kit (Solaibao Technology Co., Ltd., Beijing, Catalog No. IKA1012-1); ATP Detection Kit (Shanghai Biyun Tian Biotechnology Co., Ltd., Cat. No. S0026); TMRE Mitochondrial Membrane Potential Detection Kit (Shanghai Biyun Tian Biotechnology Co., Ltd., Cat. No. C2001S); PK Mito Mitochondrial Fluorescent Dye (Nanjing Puhai Jingshan Biotechnology Co.,

Ltd., Catalog No. PKMO-2); Calcineurin (CaN) Antibody, Dynamin-related protein 1 (Drp1) Antibody (Abcam, UK, Batch Nos. Ab282104 and Ab184247, respectively); Mitochondrial calcium uniporter (MCU) antibody (NSJ Biologics, USA, Lot No. RQ5827); Ca^{2+}/calmodulin (CaM) antibody (Proteintech, USA, Lot No. 10541-1-AP); Glyceraldehyde-3-phosphate dehydrogenase (GAPDH) antibody (Immunoway, USA, Lot No. YM3029); BCA Protein Quantification Kit (Beijing Tiandeyue Biotechnology Co., Ltd., Lot No. WB); TRIzol Total RNA Extraction Reagent (Beijing Tiangen Biochemical Technology Co., Ltd., Lot No. DP424); cDNA Synthesis SuperMix (NovoScript® Plus All-in-one 1st Strand cDNA Synthesis SuperMix) (Beijing Novobio Technology Co., Ltd., Lot No. E047-01A); Real-time Fluorescent Quantitative PCR Mix (BlazeTaq™ SYBR® Green qPCR Mix 2.0) (Gene Copoeia, USA, Lot No. QP031-S); DL2,000 DNA Marker (Beijing Qingke Biotechnology Co., Ltd., Lot No. TSJ012-100).

2.4 Instruments

Cell incubator (Thermo Fisher Scientific, USA, Model 371); Multifunctional microplate reader (BioTek, USA, Model Synergy H1); Fluorescence microscope (Nikon Corporation, Japan, Model Ti2-U); Ultracentrifuge (Thermo Scientific, USA, Model Fresco 21); Electrophoresis system (Bio-Rad, USA, Model Power Pac); High-speed electric tissue homogenizer (Fluka, Germany, Model T18); Chemiluminescence imager (Guangzhou Guangyi Biotechnology Co., Ltd., Model OI-X6 Touch); Fluorescent quantitative PCR instrument (Applied Biosystems, USA, Model QuantStudio 5); Transmission electron microscope (Hitachi, Japan, Model HT7700); Ultramicrotome (Leica, Germany, Model Leica UC7).

2.5 Methods

2.5.1 Molecular Docking of Key Active Components and Pathway-Related Proteins in YQF

Previous experimental studies using high-performance liquid chromatography identified seven bioactive components in YQF: Ginsenoside Rg1, Ginsenoside Rb1, Ginsenoside Re, Coptisine, Berberine, Ferulic acid, and Ligustilide. The CAS numbers of these seven components were entered into the PubChem database to obtain their SMILES formulas. The 2D structures of these primary bioactive components were retrieved from the PubChem database (https://pubchem.ncbi.nlm.nih.gov/) and saved in SDF format. Using Chem3D software, the structural files of these seven components underwent energy minimization and were saved in mol2 format as ligands. Core target protein IDs were identified using the UniProt protein database. The 3D structures of these key target proteins were obtained from the PDB database (https://www.rcsb.org/) and saved in PDB format. PyMOL software was used to dehydrate the target proteins and remove irrelevant ligands, with the results saved in PDB format. AutoDock Tools software was used to add hydrogen atoms to the protein receptors. Both the receptor and ligand files were converted to PDBQT format and saved. Molecular docking was performed using AutoDock Vina to identify the binding site between the protein receptor and the small-molecule ligand, and the free binding energy at this site was calculated. A lower binding energy indicates a more stable ligand-receptor binding conformation and a stronger interaction between the molecule and the target protein.

2.5.2 Cell Culture

This experiment included the following groups: Control group (293T cells), Model group (APP-PS1 cells), Donepezil group, Ginsenoside Rg1 group, Ginsenoside Rb1 group, Ginsenoside Re group, Coptisine group, Berberine group, Ferulic acid group, and Ligustilide group. Control 293T cells and Model APP-PS1 cells were cultured in 90% DMEM-H + 10% FBS + 1% P/S. All drug groups were cultured in complete medium containing the respective drug.

2.5.3 Screening of Drug Intervention Concentrations Using the CCK-8 Assay

Preliminary experiments determined the concentration range to be 0-100 μM. APP-PS1 cells in the logarithmic growth phase were seeded into 96-well plates and divided into the following groups for the formal concentration gradient experiment: blank group (culture medium only), control group (cells + complete medium), and drug intervention groups at different concentrations (cells + drug-containing medium at varying concentrations). Each group included at least six replicate wells to ensure statistical power. After 48 hours of treatment, 10 μl of CCK-8 reagent was added to each well and incubated. A microplate reader was used to measure the absorbance (OD value) of each well at 450 nm. The cell survival rate (%) for each drug concentration group was calculated using the formula: [(drug group OD value - blank group OD value) / (control group OD value - blank group OD value)] × 100%, and a dose-response curve was plotted.

2.5.4 Experimental Groups and Treatments

Experimental groups were established based on the optimal drug intervention concentrations identified through the CCK-8 assay. (1) Control group: 293T cells cultured under standard conditions; (2) Model group: APP-PS1 cells cultured under standard conditions; (3) Donepezil group: APP-PS1 cells +

Donepezil; (4) Ginsenoside Rg1 group: APP-PS1 cells + Ginsenoside Rg1; (5) Ginsenoside Rb1 group: APP-PS1 cells + Ginsenoside Rb1; (6) Ginsenoside Re group: APP-PS1 cells + Ginsenoside Re; (7) Coptisine group: APP-PS1 cells + Coptisine; (8) Berberine group: APP-PS1 cells + Berberine; (9) Ferulic acid group: APP-PS1 cells + Ferulic acid; (10) Ligustilide group: APP-PS1 cells + Ligustilide. Each group was cultured in drug-containing medium for 48 hours.

2.5.5 ATP Concentration Detection

After 48 hours of drug treatment, cells cultured in 6-well plates were lysed by adding 200 μL of lysis buffer per well on ice. The lysates were centrifuged at 4°C, 12,000×g for 5 minutes, and the supernatant was collected. To minimize variation, protein quantification kits were used to measure and equalize sample concentrations across groups, standardizing cell numbers. ATP assay working solutions and standard solutions were prepared. 100 μL of ATP assay working solution and 20 μL of standard or sample were added to each well. Luminescence was measured using a luminometer. The ATP concentration in samples was calculated based on the standard curve.

2.5.6 Mitochondrial Membrane Potential Assay

After 48 hours of drug treatment, cells cultured in 6-well plates were used for the assay. TMRE staining working solution was prepared. CCCP staining working solution was prepared and used to treat cells for 20 minutes to completely eliminate mitochondrial membrane potential as a positive control. After washing the cells and aspirating the culture medium from the 6-well plate, 1 mL of TMRE staining working solution was added to each well. The cells were incubated at 37°C in a cell culture incubator for 30 minutes. The supernatant was aspirated, and the cells were washed twice with 2 mL of pre-warmed cell culture medium, then observed under a fluorescence microscope.

2.5.7 Detection of Intracellular and Mitochondrial Calcium Ion Concentrations

2 mM Rhod-2 AM solution was mixed with 10% Pluronic F127 reagent at a 1:1 ratio to obtain the Rhod-2 mixture. The Rhod-2 mixture was diluted with Rhod-2 AM diluent to prepare a 5 μM Rhod-2 AM working solution. The working solution was added to the cells, which were then incubated at 37°C for 60 minutes. Cells were washed twice with Rhod-2 AM cell wash buffer to remove excess fluorescent probes. 300 μl of buffer was added to prepare a cell suspension, and fluorescence values were measured using a flow cytometer.

The Fura Red AM solution was diluted with HBSS to prepare a 5 μM Fura Red AM working solution. The working solution was added to the cells, which were then incubated at 37°C for 60 minutes. Cells were washed twice with HBSS buffer to remove excess fluorescent probes. 300 μl of HBSS was added to prepare a cell suspension, and fluorescence values were measured using a flow cytometer.

2.5.8 PK Mito Mitochondrial Staining

Cells were cultured in confocal microplates and subjected to drug intervention for 48 hours. 20 μL of DMSO was added to PK Mito Orange and mixed thoroughly to obtain a 250 μM stock solution. The medium was preheated to 37°C, and the PK Mito Orange stock solution was diluted 1:2000 to prepare the staining working solution. The original culture medium was aspirated from the cells. 2 ml of PK Mito Orange staining solution was added, and the cells were incubated in the incubator for 30 minutes. Cells were washed twice with pre-warmed medium. Mitochondrial imaging was observed using STED microscopy.

2.5.9 TEM Observation of Cellular Mitochondrial Ultrastructure

Cells were fixed in pre-chilled 2.5% glutaraldehyde solution at 4°C. Subsequently, the cell samples were washed three times with 0.1 M sodium phosphate buffer, then fixed with 1% osmium tetroxide (OsO_4) solution at 4°C for 2 hours to further stabilize lipid membranes and enhance electron density. Gradient alcohol dehydration was performed to ensure complete removal of water. Samples underwent gradient infiltration with a mixture of epoxy resin and acetone, followed by embedding in fresh resin. Polymerization was carried out at 60°C for 48 hours. Resin blocks were trimmed to expose target regions, and ultrathin sections (50-70 nm) were prepared and mounted on copper grids. Sections were stained with 2% uranyl acetate for 30 minutes to enhance nucleic acid and protein contrast, followed by further staining with lead citrate for 5–10 minutes to enhance membrane and organelle contrast. Stained copper grids were mounted on TEM sample holders for observation under high vacuum.

2.5.10 Western Blot Analysis for Pathway-Related Protein Expression

Protein quantification of test samples was performed using the BCA method. Separation gels were prepared based on the molecular weight of the target protein. After loading the test protein samples, electrophoresis and membrane transfer were conducted. The membrane was immersed in 3% BSA-TBST and blocked at room temperature for 30 minutes. Prepared primary antibodies were added: CaN (1:2000), MCU (1:2000), CaM (1:5000), and Drp1 (1:1000), and the membrane was incubated at room temperature for 10 minutes, then overnight at 4°C, followed by incubation at room temperature for 30 minutes the

next day. The membrane was washed with TBST. HRP-conjugated goat anti-rabbit/mouse secondary antibody was diluted 1:10,000, incubated at room temperature for 40 minutes, and the membrane was washed again. After ECL development, images were acquired and saved as "Sample," "Marker," and "Merge". ImageJ software was used to analyze the grayscale ratio of the target protein to the internal control and calculate relative expression levels.

2.5.11 Real-Time PCR Detection of Pathway-Related Protein mRNA Expression

Total RNA was extracted from samples using TRIzol® reagent. RNA quality was assessed via UV-vis spectrophotometry to determine absorbance, concentration, and purity, and denaturing agarose gel electrophoresis was performed for further analysis. Reverse transcription was conducted to synthesize cDNA. All cDNA samples were used to prepare Real-Time PCR reaction systems with the following parameters: pre-denaturation at 95°C for 5 minutes, denaturation at 95°C for 10 seconds, annealing at 60°C for 30 seconds, and extension at 72°C for 20 seconds, repeated for 40 cycles. GAPDH served as the housekeeping gene. Each sample was tested in triplicate, and the relative expression levels of target mRNAs were analyzed using the $2^{-}\Delta\Delta Ct$ method. Specific primers for the target genes were synthesized by Invitrogen (Beijing), and the primer sequences are listed in [Table 1].

Table 1. Primer sequences for the target genes

Primer	Sequence (5' to 3')	Length/bp
CaN	Upstream GTCCCAACAGACTTCTGGT	102
	Downstream CTGGACAGACGAGTTATTTGAC	
MCU	Upstream GTTGCTATCTATTCACCAGATGG	80
	Downstream CAGCTTAAAGTCATCAAGGAGG	
CaM	Upstream GTCTGTAGTGAATCCAGTACTC	80
	Downstream ACGTTCATCTAACCACTTATCC	
Drp1	Upstream GGAAATAATAAGGTGCCTGTAGG	80
	Downstream ACTGATGAACCGAAGAATGAG	
GAPDH	Upstream CACCCACTCCTCCACCTTTGA	188
	Downstream TCTCTCTTCCTCTTGTGCTCTTGC	

2.6 Statistical Methods

Statistical analysis of data was performed using GraphPad Prism 10.1.2 software. All experimental data underwent normality and homogeneity of variance tests. Results are expressed as mean ± standard deviation ($\bar{x}\pm s$). Comparisons among multiple groups were conducted using one-way analysis of variance (*One-way ANOVA*), with $P < 0.05$ indicating statistically significant differences.

3 Results

3.1 Molecular Docking Results

Using AutoDock Vina software, the active components of YQF—Ginsenoside Rg1, Ginsenoside Rb1, Ginsenoside Re, Coptisine, Berberine, Ferulic acid, and Ligustilide—were used as small-molecule ligands for molecular docking with the protein receptors PKA, CaN, CaM, MCU, NCLX, and Drp1. The default number of docking runs was set to 10. Generally, a binding energy of less than -5.0 kcal/mol indicates favorable binding between a target protein and a ligand, with lower binding energy signifying better docking. Docking results showed that Ginsenoside Rg1, Ginsenoside Rb1, Ginsenoside Re, Coptisine, Berberine, Ferulic acid, and Ligustilide all exhibited binding energies < -5.0 kcal/mol with CaN, CaM, MCU, and Drp1 proteins [Table 2], indicating strong binding potential between these seven herbal monomers and the proteins. Visualization of the docking results revealed: CaN and Drp1 proteins exhibited strong binding with Ginsenoside Rg1, Ginsenoside Rb1, Ginsenoside Re, Coptisine, Berberine, Ferulic acid, and Ligustilide, characterized by hydrogen bonds; CaM protein showed good binding with Ginsenoside Rg1, Ginsenoside Rb1, Ginsenoside Re, Coptisine, and Ferulic acid, also via hydrogen bonds; MCU exhibited good binding with Ginsenoside Rg1, Ginsenoside Rb1, Ginsenoside Re, Coptisine, Berberine, and Ferulic acid, similarly through hydrogen bonds [Fig.1].

Table 2. Molecular Docking Results of YQF Active Components with Target Proteins

Binding energy	CaN	CaM	MCU	Drp1
Ginsenoside Rg1	-9.2	-8.7	-7.8	-8.8
Ginsenoside Rb1	-10.0	-9.1	-8.0	-8.9
Ginsenoside Re	-10.1	-9.2	-7.8	-8.8
Coptisine	-9.3	-8.9	-8.4	-9.4

Berberine	-8.4	-8.4	-7.5	-7.7
Ferulic acid	-6.6	-5.0	-6.1	-6.5
Ligustilide	-6.6	-6.9	-6.5	-6.6

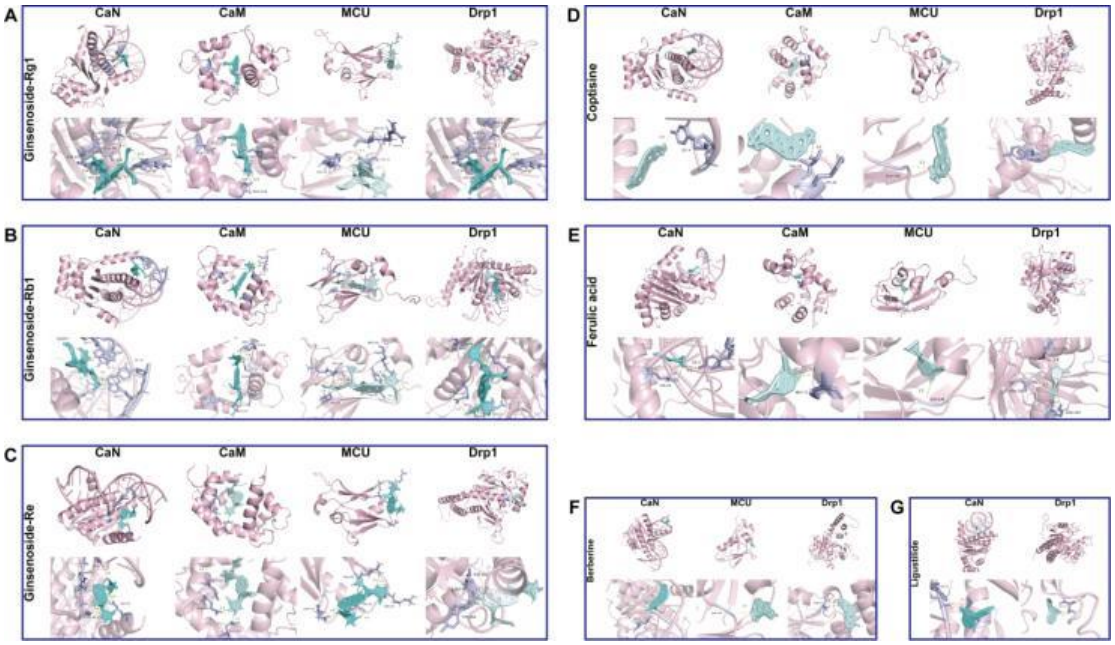

Fig. 1. Visualization of the docking results of the active components of YQF with the target molecules related to the pathways.
Note: (A-G) Visualization of the molecular docking of Ginsenoside Rg1, Ginsenoside Rb1, Ginsenoside Re, Coptisine, Ferulic acid, Berberine, and Ligustilide.

3.2 Drug Intervention Concentration

As shown in [Fig. 2], when APP-PS1 cells were treated with different concentrations of Donepezil for 48 hours, cell viability was increased compared to the control group at concentrations ranging from 0 to 1 μM. At a concentration of 1 μM, cell viability was significantly higher than that of the control group ($P<0.01$). At concentrations above 1 μM, cell viability was suppressed compared to the control group, though the difference was not significant. Intervention of APP-PS1 cells with varying concentrations of Ginsenoside Rg1, Ginsenoside Rb1, and Ginsenoside Re for 48 hours showed increased cell viability compared to the control group at Ginsenoside Rg1 concentrations of 10–20 μM ($P < 0.05$, $P < 0.01$); at a Ginsenoside Rb1 concentration of 10 μM, cell viability was higher than that of the control group ($P < 0.05$), while concentrations above 100 μM inhibited cell viability ($P < 0.05$); at a concentration of 10 μM, Ginsenoside Re increased cell viability compared to the control group ($P<0.05$), while at 200 μM, cell viability was inhibited ($P<0.05$). After 48 hours of treatment with varying concentrations of Coptisine and Berberine in APP-PS1 cells, at 5–10 μM Coptisine, cell viability was increased compared to the control group ($P<0.05$, $P<0.001$); Berberine concentrations above 100 μM resulted in lower cell viability than the normal control group ($P < 0.01$), while at a concentration of 5 μM, cell viability was higher than that of the control group, though the difference was not significant. After treating APP-PS1 cells with Ferulic acid at various concentrations for 48 hours, concentrations exceeding 100 μM resulted in significantly lower cell viability than the normal control group ($P < 0.01$), while at a concentration of 10 μM, cell viability was higher than that of the control group, but the difference was not significant. After 48 hours of treatment with different concentrations of Ligustilide in APP-PS1 cells, the 50 μM concentration resulted in significantly higher cell viability than the control group ($P<0.0001$), with a statistically significant difference. Therefore, the intervention concentrations for each drug were determined as follows: Donepezil (1 μM), Ginsenoside Rg1 (20 μM), Ginsenoside Rb1 (10 μM), Ginsenoside Re (10 μM), Coptisine (5 μM), Berberine (5 μM), Ferulic acid (10 μM), Ligustilide (50 μM).

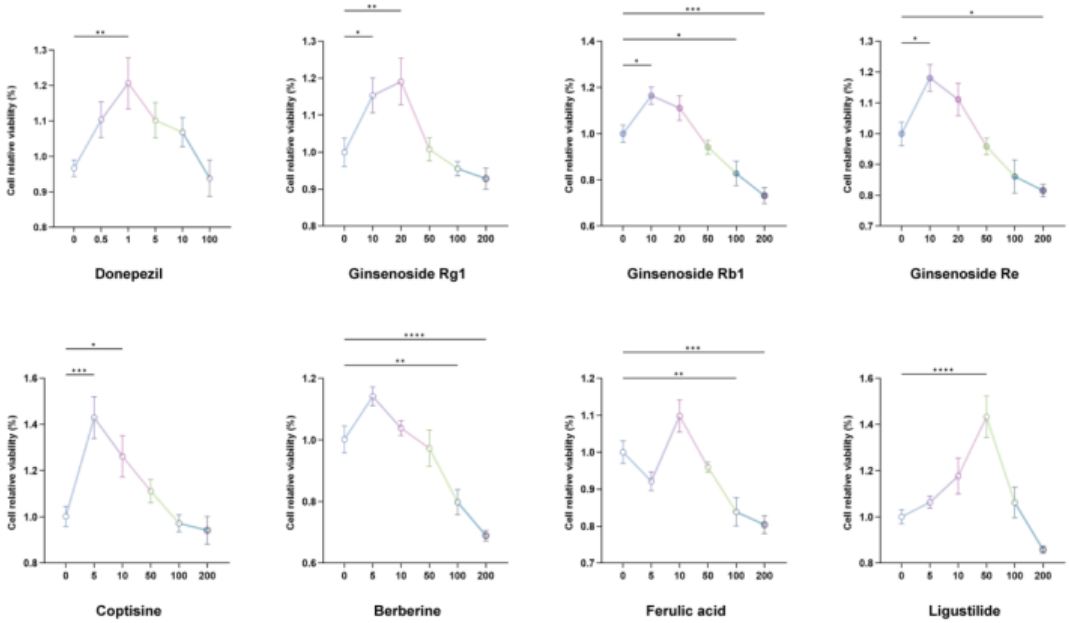

Fig. 2. The effect of different concentrations of YQF active components on the viability of APP-PS1 cells (n=6). Note: Compared with the control group (with drug concentration of 0), $^{*}P<0.05$; $^{**}P<0.01$; $^{***}P<0.001$; $^{****}P<0.0001$.

3.3 ATP Content Detection

Intracellular ATP concentrations were measured using an ATP assay kit. Results [Fig. 3A-B] showed that compared to the Control group, intracellular ATP concentrations were significantly reduced in the APP-PS1 Model group ($P<0.001$), indicating mitochondrial dysfunction in AD model cells. Compared to the Model group, the Donepezil, Ginsenoside Rg1, Ginsenoside Rb1, Ginsenoside Re, Ferulic acid, and Ligustilide groups showed significantly increased intracellular ATP concentrations ($P<0.05$, $P<0.01$), indicating that Donepezil and the active components of YQF effectively improved the reduced ATP concentration caused by mitochondrial dysfunction in APP-PS1 model cells.

3.4 Mitochondrial Membrane Potential Detection

Mitochondrial membrane potential was measured using the TMRE assay kit. Results showed [Fig. 3C-D] that compared to the Control group, cells in the APP-PS1 Model group exhibited reduced fluorescence intensity and significantly decreased mitochondrial membrane potential ($P < 0.01$), indicating impaired energy metabolism in AD model cells. Compared to the Model group, mitochondrial membrane potential was increased in the Donepezil, Ginsenoside Rg1, Ginsenoside Re, Ferulic acid, and Ligustilide groups ($P<0.05$, $P<0.01$). This demonstrates that Donepezil and the active components of YQF effectively improve the reduced mitochondrial membrane potential caused by mitochondrial dysfunction in APP-PS1 model cells.

3.5 Detection of Intracellular and Mitochondrial Ca^{2+} Concentrations

Intracellular Ca^{2+} concentrations were measured using the Fura Red AM calcium fluorescent probe, while mitochondrial Ca^{2+} concentrations were detected with the Rhod-2 AM fluorescent probe. Results showed [Fig. 3E-H] that compared with the Control group, both intracellular and mitochondrial Ca^{2+} fluorescence intensity was significantly increased in the APP-PS1 Model group ($P<0.001$, $P<0.0001$), indicating Ca^{2+} overload in both cytoplasmic and mitochondrial compartments of AD model cells. Compared with the Model group, Ca^{2+} levels in both cytoplasmic and mitochondrial compartments were reduced in the Donepezil group ($P < 0.01$, $P < 0.0001$). Additionally, the Ginsenoside Rg1, Ginsenoside Rb1, Ginsenoside Re, Berberine, Ferulic acid, and Ligustilide groups showed significantly lower intracellular and mitochondrial Ca^{2+} levels than the Model group ($P < 0.05$, $P < 0.01$). This indicates that Donepezil and the active components of YQF effectively mitigate Ca^{2+} overload caused by mitochondrial dysfunction in APP-PS1 model cells.

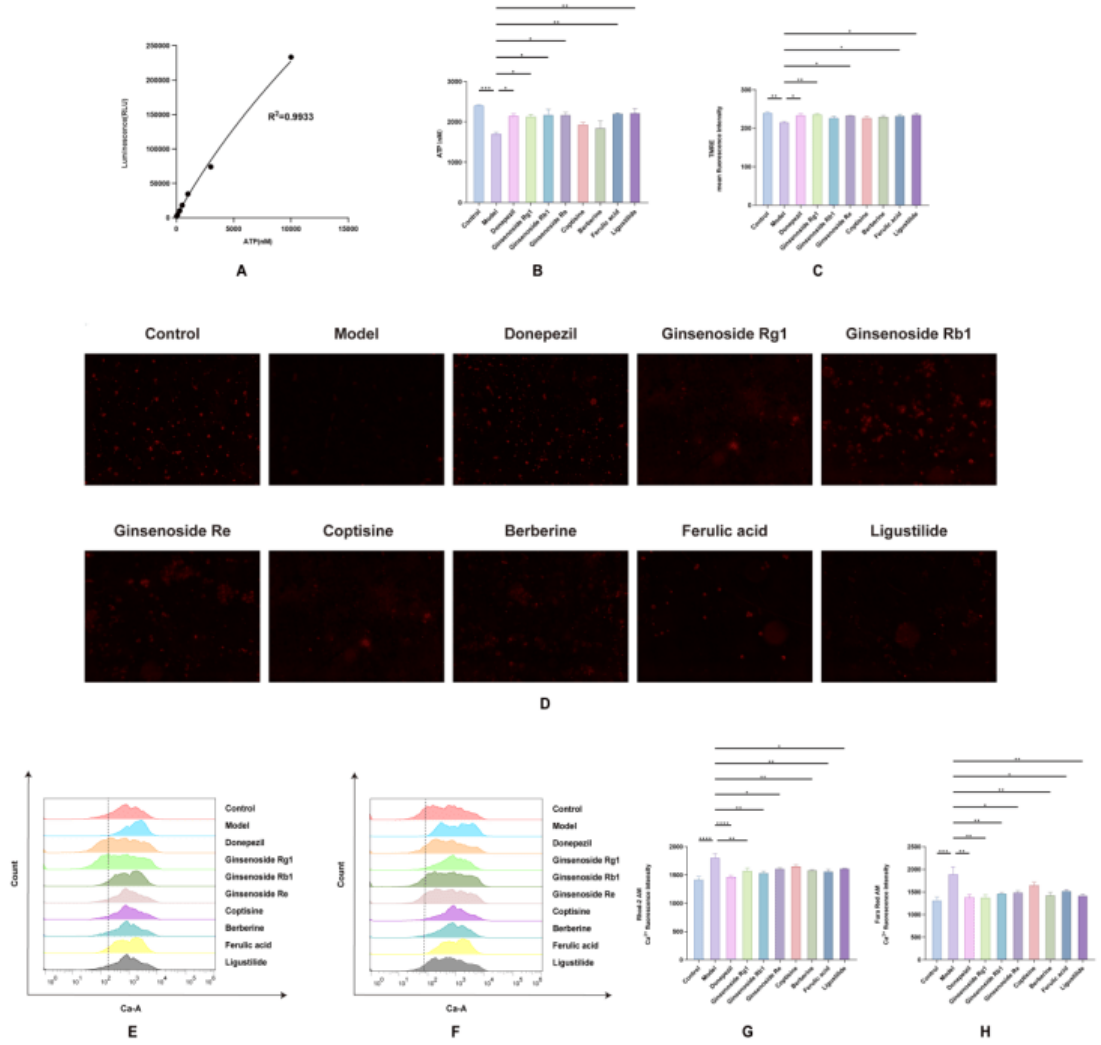

Fig. 3. The effect of active components in YQF on mitochondrial function in APP-PS1 cells (n=5). Note: (A) ATP concentration standard curve; (B) The ATP concentrations of each group of cell samples; (C) Quantitative analysis of mitochondrial membrane potential fluorescence in each group of cells; (D) The typical image of TMRE staining; (E) Rhod-2 AM Fluorescent Probe Detection of Mitochondrial Ca^{2+} Concentration Flow Cytometry Stacked Graph; (F) Fura Red AM Fluorescent Probe Detection of Intracellular Ca^{2+} Concentration Flow Cytometry Stacked Graph; (G) Quantitative analysis of mitochondrial Ca^{2+} levels; (H) Quantitative analysis of intracellular Ca^{2+} levels. Data were expressed as the Mean ± SEM. $^{*}P < 0.05$, $^{**}P < 0.01$, $^{***}P < 0.001$, vs. Model group.

3.6 PK Mito Mitochondrial Staining

Cells were stained with PK Mito Orange to visualize mitochondria, and mitochondrial morphology was observed using STED imaging. As shown in [Fig. 4A], the results indicated that mitochondria in the Control group 293T cells predominantly exhibited elliptical or rod-like shapes with relatively regular alignment, showing no obvious swelling or vacuolation. In contrast, mitochondria in the Model group APP-PS1 cells demonstrated altered structural morphology, characterized by swollen and deformed shapes, shortened lengths, fragmentation, irregular sizes, and abnormal spatial distribution. Following treatment with Donepezil and the active components of YQF, mitochondrial morphology was improved in the Donepezil, Ginsenoside Rg1, Ginsenoside Rb1, Ginsenoside Re, Coptisine, Berberine, Ferulic acid, and Ligustilide groups compared to the Model group. Mitochondrial swelling was reduced, with cells predominantly exhibiting rod-shaped morphology and relatively regular arrangement. Analysis of Mean Branch Length (μm) using ImageJ's Mitochondria Analyzer plugin revealed [Fig. 4B] that compared to the Control group, cells in the APP-PS1 Model group exhibited significantly shorter Mean Branch Length ($P < 0.0001$). This indicates pronounced mitochondrial damage in AD model cells, characterized by altered morphology, fragmentation, shortening, and swelling. Compared to the Model group, cells treated with Donepezil, Ginsenoside Rg1, Ginsenoside Rb1, Ginsenoside Re, Coptisine, Berberine, Ferulic acid, and Ligustilide exhibited significantly longer Mean Branch Length ($P < 0.0001$), with statistically

significant differences. This indicates that Donepezil and the active components of YQF effectively improve mitochondrial dysfunction-induced morphological alterations, swelling, and fragmentation in APP-PS1 model cells.

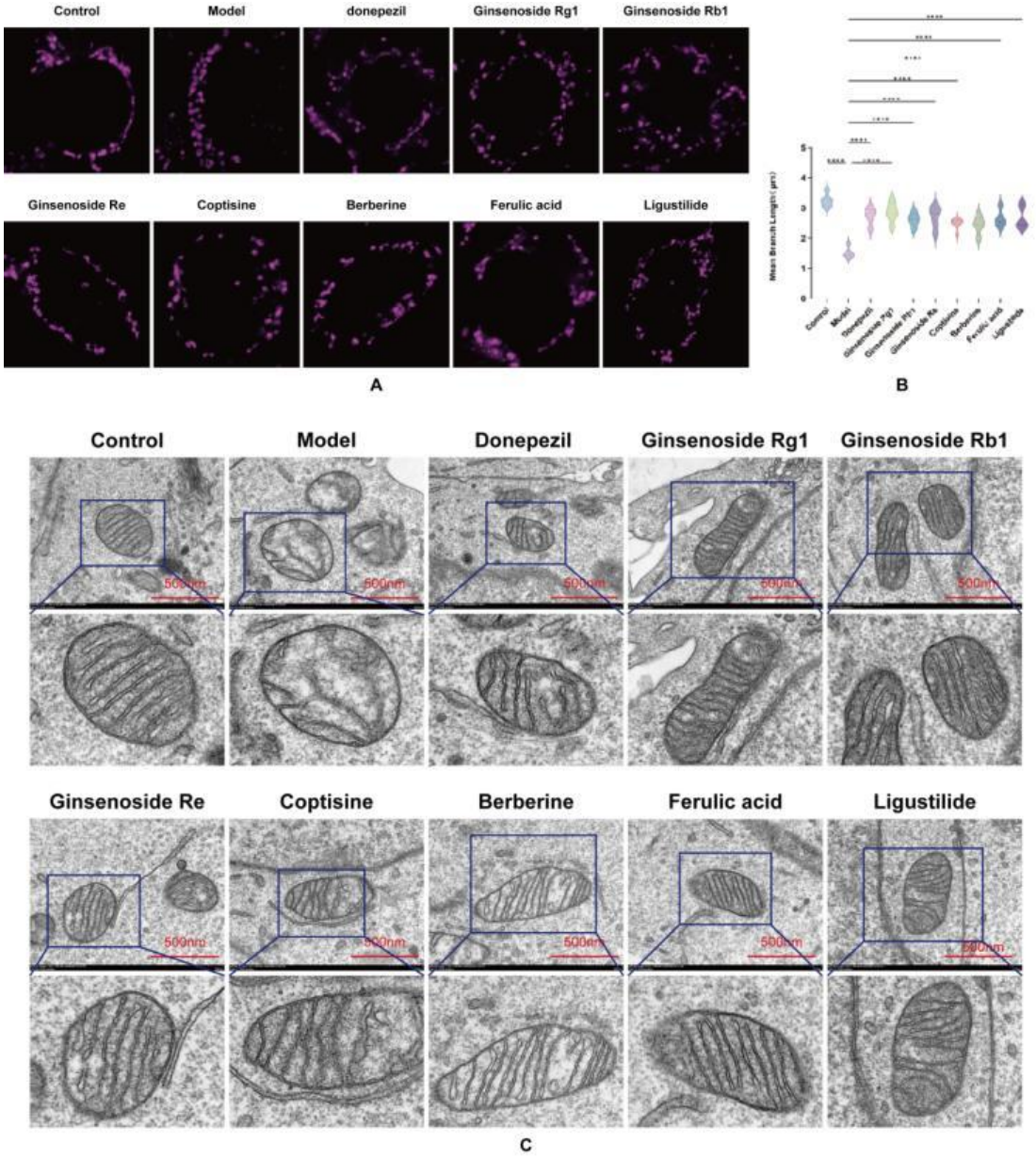

Fig. 4. The effect of YQF active components on mitochondrial morphology and ultrastructure of APP-PS1 cells (n=5). Note: (A) PK Mito Orange Mitochondrial Staining Typical Image (STED, Scale bar = 5 μm); (B) Quantitative Analysis of Mitochondrial Mean Branch Length; (C) Mitochondrial Subcellular Structure (40,000×, bar=500 nm). Data were expressed as the Mean ± SEM. $^{*}P < 0.05$, $^{**}P < 0.01$, $^{***}P < 0.001$, vs. Model group.

3.7 TEM Observation of Cellular Mitochondrial Ultrastructure

Transmission electron microscopy (TEM) was used to observe alterations in the subcellular structure of mitochondria in cells from various drug treatment groups. Results showed [Fig. 4C] that mitochondria in Control group 293T cells predominantly exhibited oval or elongated rod-like shapes with intact, continuous inner and outer membrane structures. They displayed uniform morphology and size with regular distribution. Mitochondrial cristae were neatly arranged in typical layered or tubular patterns, with no swelling or vacuolation observed. Mitochondrial matrix density was uniform, with only a few lysosomes and autophagosomes visible. In contrast, mitochondria in APP-PS1 model cells exhibited pathological alterations: swollen and deformed morphology, blurred outer membrane structure, irregular size, and abnormal spatial distribution. Mitochondrial cristae showed fragmentation, dissolution, or disorganized arrangement, with reduced layered features and accompanying vacuolization. Following treatment with Donepezil and the active components of YQF, mitochondrial ultrastructure was improved

in the Donepezil, Ginsenoside Rg1, Ginsenoside Rb1, Ginsenoside Re, Coptisine, Berberine, Ferulic acid, and Ligustilide groups compared to the model group. This improvement was characterized by enhanced membrane clarity and relatively intact cristae structures. These results indicate that the active components of YQF exert a reparative effect on mitochondrial structural damage in AD model cells

3.8 Western Blot Analysis for Detection of Pathway-Related Protein Expression

Western blot analysis was performed to detect the expression of CaN, CaM, MCU, and Drp1 proteins in cells. Compared with the Control group, the APP-PS1 Model group exhibited increased expression of CaN, CaM, MCU, and Drp1 ($P<0.05$, $P<0.01$). Compared with the Model group, the Donepezil group showed decreased expression of CaN, CaM, MCU, and Drp1 proteins ($P < 0.05$). The Ginsenoside Rg1 group exhibited decreased expression of CaN, CaM, and MCU proteins ($P < 0.05$), while the Ginsenoside Rb1 group demonstrated decreased CaN protein expression ($P < 0.05$). Cells in the Ginsenoside Re group showed decreased CaN and Drp1 protein expression ($P<0.05$), cells in the Berberine group exhibited decreased CaN, CaM, MCU, and Drp1 protein expression ($P<0.05$), cells in the Ferulic acid group showed decreased expression of CaN, CaM, and Drp1 proteins ($P < 0.05$, $P < 0.01$), cells in the Ligustilide group exhibited decreased expression of CaN, CaM, MCU, and Drp1 proteins ($P<0.05$, $P<0.01$), while cells in the Coptisine group showed no significant differences in protein expression [Fig. 5A-E].

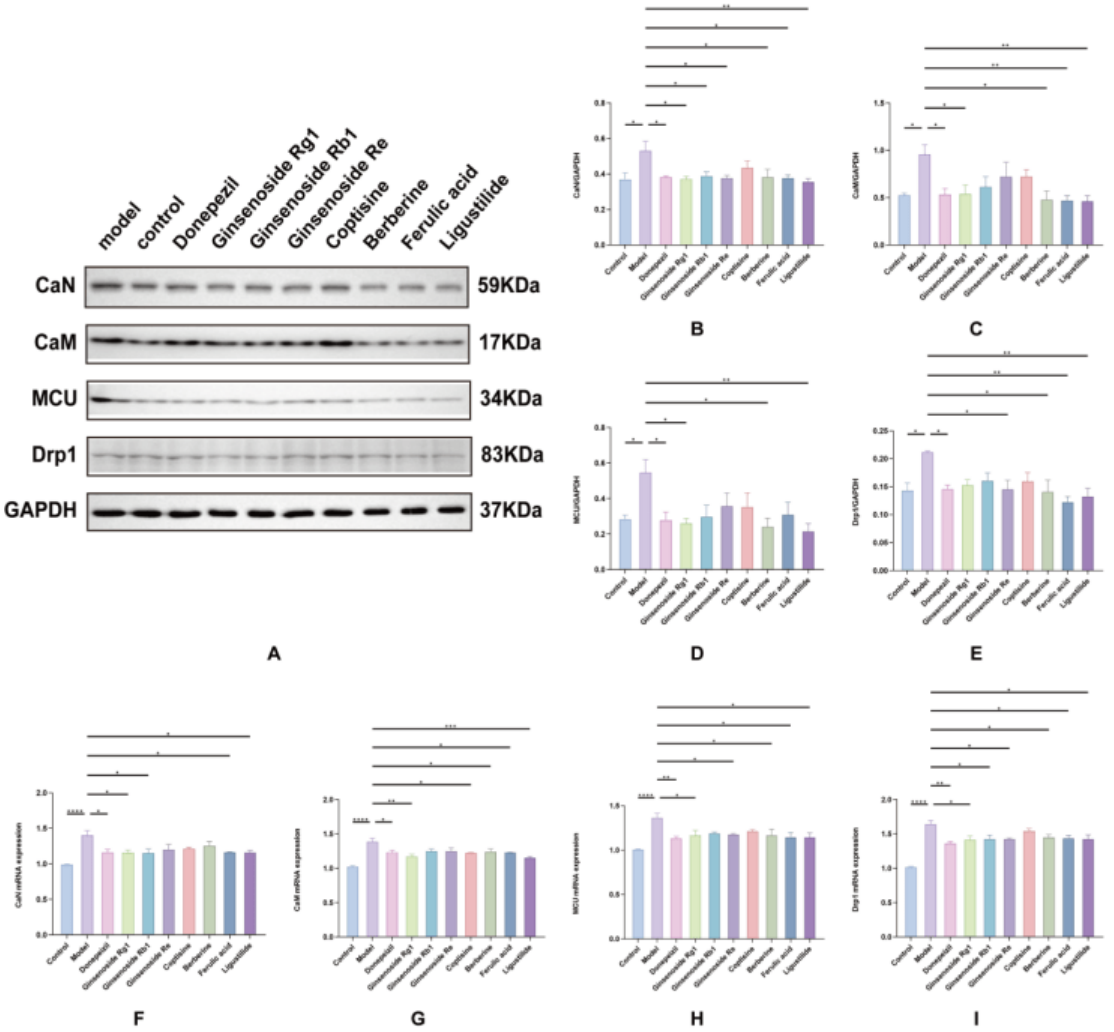

Fig. 5. The effect of YQF active components on the expression of CaN, CaM, MCU, Drp1 proteins and mRNA in APP-PS1 cells (n=5). Note: (A) Representative Western blot patterns of CaN, CaM, MCU, and Drp1 proteins in cells; (B-E) Quantitative analysis of CaN, CaM, MCU, and Drp1 protein expression in cells. (F-I) Quantitative analysis of CaN, CaM, MCU, and Drp1 mRNA expression in cells. Data were expressed as the Mean ± SEM. *$P < 0.05$, **$P < 0.01$, ***$P < 0.001$, vs. Model group.

3.9 Real-Time PCR Detection of Pathway-Related Protein mRNA Expression

Real-time PCR was used to detect the expression levels of PKA, CaN, CaM, MCU, NCLX, and Drp1 mRNA in each group of cells. Compared with the Control group, the APP-PS1 Model group showed

increased expression of CaN, CaM, MCU, and Drp1 mRNA ($P<0.0001$). Compared with the Model group, the Donepezil and Ginsenoside Rg1 groups showed decreased mRNA expression of CaN, CaM, MCU, and Drp1 ($P < 0.05$, $P < 0.01$), while the Ginsenoside Rb1 group exhibited reduced CaN and Drp1 mRNA expression ($P < 0.05$). The Ginsenoside Re group showed decreased MCU and Drp1 mRNA expression ($P<0.05$), the Coptisine group exhibited decreased CaM mRNA expression ($P<0.05$), the Berberine group showed decreased CaM, MCU, and Drp1 mRNA expression ($P<0.05$), the Ferulic acid group exhibited decreased CaN, CaM, MCU, and Drp1 mRNA expression ($P<0.05$), and the Ligustilide group demonstrated decreased CaN, CaM, MCU, and Drp1 mRNA expression ($P<0.05$, $P<0.001$) [Fig. 5F-I].

4 Discussion

4.1 Pathogenesis of AD

An essential biological characteristic of cellular aging is mitochondrial dysfunction, a degenerative change that affects many different cells in the central nervous system, such as neurons, astrocytes, and microglia [14]. Ca^{2+} regulates neuronal growth, synaptic plasticity, and cognitive function. According to Khachaturian's hypothesis, Ca^{2+} homeostasis imbalance can impair neuronal function and lead to the onset of Alzheimer's disease (AD) [15]. Mitochondria, serving as dual functional hubs for ATP synthesis and Ca^{2+} storage, dynamically respond to cellular energy demands and apoptotic signals by regulating Ca^{2+} uptake, storage, and efflux mechanisms. Mitochondrial dysfunction impairs ATP synthesis, inhibits Na^{+}-Ca^{2+} exchange, and causes intracellular Ca^{2+} overload, disrupting Ca^{2+} homeostasis [16]. Elevated intracellular Ca^{2+} levels in neurons alter mitochondrial membrane potential, affecting mitochondrial metabolism, ATP production, and neurotransmitter release at the synaptic level, thereby exacerbating neurodegeneration [16]. Chronic Ca^{2+} overload triggers expression of apoptosis-related proteins in the brain [17], further impairing cognitive function. Ca^{2+} fluorescence detection revealed significantly enhanced intracellular and mitochondrial Ca^{2+} fluorescence intensity in the APP-PS1 Model group compared to the Control group, indicating Ca^{2+} overload in both cellular and mitochondrial compartments of the AD model. Following intervention with Donepezil, Ginsenoside Rg1, Ginsenoside Rb1, Ginsenoside Re, Berberine, Ferulic acid, and Ligustilide, Ca^{2+} levels in both APP-PS1 cells and mitochondria decreased. This demonstrates that the active ingredients of YQF can effectively regulate calcium homeostasis, improve mitochondrial dysfunction, and thereby exert anti-AD effects.

Mitochondria maintain their normal structure and physiological functions through continuous processes of fission and fusion, a dynamic phenomenon defined as mitochondrial dynamics. Under physiological conditions, mitochondria sustain their normal morphology, function, and distribution via a fission-fusion equilibrium. Excessive fission causes mitochondrial fragmentation and malfunction when this balance is upset. Mitochondrial fragmentation is observed in brain tissues of AD patients and animal models [18], indicating a kinetic imbalance characterized by enhanced fission and impaired fusion during AD pathogenesis [19]. This imbalance may serve as an initiating factor for mitochondrial dysfunction and neuronal injury. Drp1, a key regulator of mitochondrial fission, interacts with Aβ and p-Tau to induce mitochondrial dysfunction [20]. Encoded by the DNM1L gene, Drp1 contracts and cleaves mitochondria in a GTPase-dependent manner [21] and is highly enriched in the central nervous system. Both clinical and basic studies have revealed significantly elevated Drp1 activity in cortical tissues from both AD patients and AD mouse models [22]. The biological activity of Drp1 protein is finely regulated by multiple post-translational modification mechanisms, with phosphorylation being the most prevalent. Ser637 serves as a critical phosphorylation site. The phosphorylation and dephosphorylation states at Ser637 determine the activation and inactivation of Drp1, constituting a core molecular mechanism regulating the balance between mitochondrial fission and fusion. Western blot and real-time PCR analyses revealed increased Drp1 protein and mRNA expression in Model group cells compared to the Control group, indicating enhanced mitochondrial fission in AD cells. Following intervention with Donepezil and the active ingredients of YQF, Drp1 protein and mRNA expression decreased in Model group cells. This demonstrates that the active ingredients of YQF can suppress Drp1 protein expression, inhibit mitochondrial fission, and thereby improve mitochondrial dysfunction.

4.2 Pharmacological Mechanism of YQF in Treating Alzheimer's Disease

The pathogenesis of Alzheimer's disease (AD) is multifaceted, with deficiency-depletion serving as the fundamental basis for disease onset. During disease progression, pathological products such as blood stasis and phlegm-turbidity accumulate, with stasis-toxin damaging the cerebral collaterals [23]. Based on an in-depth understanding of AD's “deficiency-depletion and stasis-toxin” pathogenesis, Professor Zhou Wenquan, drawing upon extensive clinical experience, proposed the therapeutic principle of tonifying deficiency-depletion while promoting blood circulation, resolving stasis, and detoxifying. Guided by this therapeutic principle, the “Yizhi Qingxin Formula” was developed. This decoction combines three

Chinese herbs—Ginseng, Coptis, and Ligusticum—in a 9:5:6 ratio. Ginseng fortifies qi, consolidates the foundation, nourishes the five viscera, calms the spirit, and enhances cognition; Coptis rhizome clears heat, purges fire, detoxifies, and strengthens the spleen and stomach; Ligusticum root promotes blood circulation and removes blood stasis while also transporting the formula upward to deliver the herbs directly to the cerebral lesion [24]. Active ingredients in ginseng, such as ginsenosides, exhibit significant neuroprotective effects. By regulating neuroimmune inflammatory responses, mitigating oxidative stress damage, enhancing synaptic plasticity, and safeguarding mitochondrial functional integrity, these compounds effectively alleviate neurological symptoms including cognitive decline [25]. Berberine, the primary component of Coptis, has been demonstrated to intervene in the pathological deposition of β-amyloid and exhibit neuroprotective functions [25]. The active component ligustilide in Chuanxiong inhibits neuroinflammatory cascades by downregulating inflammatory factor expression, while ferulic acid significantly antagonizes β-amyloid-induced neuronal toxicity [26]. Consequently, the Yizhi Qingxin Formula exhibits neuroprotective effects and demonstrates efficacy against AD.

Previous studies have demonstrated that the Yizhi Qingxin Formula improves AD by regulating the PKA/CaN pathway [13]. High-performance liquid chromatography identified the primary active ingredients of the formula as ginsenoside Rg1, ginsenoside Re, ginsenoside Rb1, berberine, palmatine, ligustilide, and ferulic acid [12]. Integrating modern pharmacological research, ginsenoside Rb1 can upregulate PKA expression [26], inhibit CaN signaling [27], and influence elevated Drp1 protein levels to suppress mitochondrial fission abnormalities [28]; Ginsenoside Re inhibits L-type Ca^{2+} channels, suppressing excessive Ca^{2+} influx [26]; Berberine downregulates PKA protein levels by inhibiting the PKA signaling pathway [28] while simultaneously suppressing the transcriptional activity of CaN pathway-related genes [29], effectively inhibiting Drp1-induced abnormal mitochondrial fission and thereby exerting an anti-apoptotic effect; Ferulic acid targets PKA to reduce CaN expression in brain tissue of AD model mice and maintains the dynamic equilibrium of mitochondrial fission and fusion by regulating Drp1 phosphorylation status [30].

4.3 Mechanism of Action of YQF Active Ingredients in Treating AD

In Alzheimer's disease (AD) models, ginsenoside Rg1 has multi-target neuroprotective benefits [31]. It reduces Aβ production and deposition by lowering APP levels and BACE1 expression, while also inhibiting tau hyperphosphorylation, thereby improving learning and memory functions. Its mechanism of action involves attenuating oxidative stress, suppressing inflammatory responses, promoting autophagy and microglia-mediated Aβ clearance, and exerting protective effects by regulating signaling pathways such as BDNF-TrkB and Akt/ERK [32]. Structurally, Rg1 belongs to the protopanaxatriol (PPT) type of ginsenosides, while Rb1 is a protopanaxadiol (PPD) type. Both enhance synaptic plasticity and exhibit neuroprotective properties including anti-inflammatory, antioxidant, and anti-apoptotic effects [33,34]. Furthermore, ginsenoside Re demonstrates inhibitory effects on Aβ production and neuroprotective actions in AD models by activating PPARγ, inhibiting BACE1, and regulating ROS-dependent ASK-1/JNK/Bax and NRF2 antioxidant pathways [35,36].

In traditional Chinese medicine theory, Coptis chinensis is used to treat dementia due to its efficacy in clearing heat, drying dampness, purging fire, and detoxifying, thereby mitigating damage to cerebral vessels caused by internal toxins and heat pathogens [37]. Modern research confirms that its primary active component, berberine (BBR), exhibits antioxidant, anti-inflammatory, and neuroprotective effects. It can improve memory and learning in AD mice by penetrating the blood-brain barrier. Its mechanisms of action include promoting mitochondrial autophagy to reduce Aβ production, inhibiting excessive phosphorylation of tau protein [38], regulating Aβ-induced neuroinflammation and oxidative stress via the PI3K/AKT and NFκB pathways [39], and alleviating mitochondrial dysfunction by maintaining mitochondrial membrane potential and increasing mitochondrial density and length [40]. Animal studies further demonstrate that BBR inhibits amyloid plaque deposition and neurofibrillary tangle formation, significantly improving memory and cognitive impairments [41].

The active component ligustilide in Chuanxiong (Ligusticum chuanxiong) exerts protective effects against $A\beta_{25-35}$-induced neurotoxicity, offering a novel therapeutic strategy for AD [42]. Ligustilide can cross the blood-brain barrier, regulate mitochondrial homeostasis, reduce intracerebral Aβ levels in APP/PS1 animal models, and restore synaptic structure, thereby improving memory deficits [43]. Furthermore, LIG exhibits antioxidant activity and improves mitochondrial and neurological function in SAMP8 mice, suggesting its potential as an anti-dementia agent [44]. Another active component, ferulic acid (FA), reduces Aβ deposition and IL-1β levels in the frontal cortex of APP/PS1 transgenic mice while enhancing novel object recognition, providing theoretical support for its therapeutic application in AD [45].

4.4 The active ingredients of YQF treat AD by regulating CaN, CaM, MCU and Drp1

A major pathogenic characteristic in the early stages of Alzheimer's disease (AD) is mitochondrial malfunction, which is primarily caused by disruption of mitochondrial Ca^{2+} homeostasis and kinetic imbalance. Therefore, improving mitochondrial dysfunction can reduce synaptic and neuronal damage, thereby inhibiting AD progression. The mitochondrial calcium uncoupler (MCU) primarily mediates Ca^{2+} influx, and intracellular Ca^{2+} overload activates calcium-activated nucleoside synthase (CaN) [46]. CaN is a Ca^{2+}-sensitive serine/threonine phosphatase highly enriched in neurons, activated by CaM-formed complexes. Abnormal CaN activation leads to dendritic spine loss and synaptic damage, ultimately causing neuronal process degeneration and reduced synapse numbers [47]. Inhibiting CaN activity improves mitochondrial function. When PKA catalyzes the phosphorylation of Drp1, it significantly inhibits its GTPase activity, suppressing Drp1 function, hindering mitochondrial fission, and promoting mitochondrial fusion. Conversely, the dephosphorylation reaction mediated by CaN activates Drp1 activity, enhancing mitochondrial fission and leading to mitochondrial fragmentation [48].

Our findings reveal that the active ingredients of Yizhi Qingxin Formula—Ginsenoside Rg1, Ginsenoside Rb1, Ginsenoside Re, Coptisine, Berberine, Ferulic acid, and Ligustilide—improve mitochondrial dysfunction in AD models by regulating the expression of CaN, CaM, MCU, and Drp1 proteins. Morphological observations indicate that treatment with YQF's active ingredients improves mitochondrial morphology compared to AD model cells, characterized by enhanced membrane structure clarity and relatively intact cristae architecture. Concurrently, ATP content and mitochondrial membrane potential are both restored. These components exert their effects by downregulating CaN, CaM, MCU, and Drp1 protein expression to modulate calcium homeostasis and mitochondrial dynamic homeostasis, thereby improving mitochondrial dysfunction. This finding is consistent with previous studies [49]. The concurrent downregulation of CaN, MCU, and Drp1 mRNA expression aligns with pathway protein expression patterns. Elevated Drp1 protein levels in model group cells indicate enhanced mitochondrial fission. The active ingredients of YQF regulate mitochondrial fission by inhibiting Drp1 protein, thereby maintaining mitochondrial dynamic equilibrium. Concurrently, increased expression of MCU, CaN, and CaM proteins in model group cells suggests mitochondrial calcium overload in AD model cells. The active ingredients of YQF modulate calcium homeostasis by downregulating CaN, CaM, and MCU proteins.

5 Conclusion

In summary, the active ingredients of YQF regulate mitochondrial Ca^{2+} homeostasis and mitochondrial dynamics in APP-PS1 cells by downregulating the expression of CaN, CaM, MCU, Drp1 proteins and their corresponding mRNAs. This improves mitochondrial function and alleviates mitochondrial pathological damage in AD cells. This indicates that the active ingredients of YQF—Ginsenoside Rg1, Ginsenoside Rb1, Ginsenoside Re, Coptisine, Berberine, Ferulic acid, and Ligustilide—exhibit therapeutic efficacy in treating AD, providing a theoretical basis for developing AD treatment strategies based on traditional Chinese medicine components.

Abbreviations

Aβ	β-amyloid
AD	Alzheimer’s disease
APP-PS1	Amyloid Precursor Protein- Presenilin 1
YQF	Yizhi Qingxin Formula
PKA	Protein Kinase A
CaN	Calcineurin
CaM	Calmodulin
MCU	Mitochondrial calcium uniporter
NCLX	Sodium/Calcium/Lithium Exchanger
Drp1	Dynamin-related protein 1
TEM	Transmission Electron Microscopy
NMDA	N-methyl-D-aspartate
CCK8	Cell Counting Kit-8

References

[1] Zheng Q, Wang X. Alzheimer's disease: insights into pathology, molecular mechanisms, and therapy. Protein Cell. 2025;16(2):83-120. https://doi.org/10.1093/procel/pwae026

[2] Twarowski B, Herbet M. Inflammatory Processes in Alzheimer's Disease-Pathomechanism, Diagnosis and Treatment: A Review.

Int J Mol Sci. 2023;24(7):6518. Published 2023 Mar 30. https://doi.org/10.3390/ijms24076518
[3] Scheltens P, De Strooper B, Kivipelto M, et al. Alzheimer's disease. Lancet. 2021;397(10284):1577-1590. https://doi.org/10.1016/s0140-6736(20)32205-4
[4] Singh R, Rai S, Bharti PS, et al. Circulating small extracellular vesicles in Alzheimer's disease: a case-control study of neuro-inflammation and synaptic dysfunction. BMC Med. 2024;22(1):254. Published 2024 Jun 20. https://doi.org/10.1186/s12916-024-03475-z
[5] Greenberg BD. Alzheimer's & Dementia-Translational Research and Clinical Interventions: Strategic vision and expanded guidelines for manuscript submissions. Alzheimers Dement (N Y). 2022;8(1):e12277. Published 2022 Mar 15. https://doi.org/10.1002/trc2.12277
[6] Monzio Compagnoni G, Di Fonzo A, Corti S, Comi GP, Bresolin N, Masliah E. The Role of Mitochondria in Neurodegenerative Diseases: the Lesson from Alzheimer's Disease and Parkinson's Disease. Mol Neurobiol. 2020;57(7):2959-2980. https://doi.org/10.1007/s12035-020-01926-1
[7] Morton H, Kshirsagar S, Orlov E, et al. Defective mitophagy and synaptic degeneration in Alzheimer's disease: Focus on aging, mitochondria and synapse. Free Radic Biol Med. 2021;172:652-667. https://doi.org/10.1016/j.freeradbiomed.2021.07.013
[8] Reddy PH, Manczak M, Kandimalla R. Mitochondria-targeted small molecule SS31: a potential candidate for the treatment of Alzheimer's disease. Hum Mol Genet. 2017;26(8):1483-1496. https://doi.org/10.1093/hmg/ddx052
[9] Li H, Deng B, Lin M, Lai L, Zhao J, Li Y. HDAC3 Epigenetic Suppression by Electroacupuncture Restores AMPA Receptor Function and Synaptic Plasticity in Alzheimer's Disease Models. Neuromolecular Med. 2025;27(1):72. https://doi.org/10.1007/s12017-025-08892-8
[10] Klemmensen MM, Borrowman SH, Pearce C, Pyles B, Chandra B. Mitochondrial dysfunction in neurodegenerative disorders. Neurotherapeutics. 2024;21(1):e00292. https://doi.org/10.1016/j.neurot.2023.10.002
[11] Wang F, Feng J, Yang Y, et al. The Chinese herbal formula Fuzheng Quxie Decoction attenuates cognitive impairment and protects cerebrovascular function in SAMP8 mice. Neuropsychiatr Dis Treat. 2018;14:3037-3051. https://doi.org/10.2147/ndt.s175484
[12] Yang Y, Jia X, Feng J, et al. Fuzheng Quxie Decoction Ameliorates Learning and Memory Impairment in SAMP8 Mice by Decreasing Tau Hyperphosphorylation. Evid Based Complement Alternat Med. 2017;2017:5934254. https://doi.org/10.1155/2017/5934254
[13] Guo X, Liu J, Shi D, et al. Study on Mechanism of Yizhi Qingxin Formula Regulating PKA/CaN Pathway and Improving Cognitive Function in Alzheimer's Disease Model Mice [J/OL]. Chinese Journal of Experimental Traditional Medical Formulae, 1-15. https://doi.org/10.13422/j.cnki.syfjx.20252009
[14] Donato L, Mordà D, Scimone C, Alibrandi S, D'Angelo R, Sidoti A. From powerhouse to regulator: The role of mitoepigenetics in mitochondrion-related cellular functions and human diseases. Free Radic Biol Med. 2024;218:105-119. https://doi.org/10.1016/j.freeradbiomed.2024.03.025
[15] Alzheimer's Association Calcium Hypothesis Workgroup. Calcium Hypothesis of Alzheimer's disease and brain aging: A framework for integrating new evidence into a comprehensive theory of pathogenesis. Alzheimers Dement. 2017;13(2):178-182.e17. https://doi.org/10.1016/j.jalz.2016.12.006
[16] Calvo-Rodriguez M, Hou SS, Snyder AC, et al. Increased mitochondrial calcium levels associated with neuronal death in a mouse model of Alzheimer's disease. Nat Commun. 2020;11(1):2146. Published 2020 May 1. https://doi.org/10.1038/s41467-020-16074-2
[17] Melo Dos Santos LS, Trombetta-Lima M, Eggen B, Demaria M. Cellular senescence in brain aging and neurodegeneration. Ageing Res Rev. 2024;93:102141. https://doi.org/10.1016/j.arr.2023.102141
[18] Frye RE, Rincon N, McCarty PJ, Brister D, Scheck AC, Rossignol DA. Biomarkers of mitochondrial dysfunction in autism spectrum disorder: A systematic review and meta-analysis. Neurobiol Dis. 2024;197:106520. https://doi.org/10.1016/j.nbd.2024.106520
[19] Bhatti JS, Kaur S, Mishra J, et al. Targeting dynamin-related protein-1 as a potential therapeutic approach for mitochondrial dysfunction in Alzheimer's disease. Biochim Biophys Acta Mol Basis Dis. 2023;1869(7):166798. https://doi.org/10.1016/j.bbadis.2023.166798
[20] Medala VK, Gollapelli B, Dewanjee S, Ogunmokun G, Kandimalla R, Vallamkondu J. Mitochondrial dysfunction, mitophagy, and role of dynamin-related protein 1 in Alzheimer's disease. J Neurosci Res. 2021;99(4):1120-1135. https://doi.org/10.1002/jnr.24781
[21] Baek SH, Park SJ, Jeong JI, et al. Inhibition of Drp1 Ameliorates Synaptic Depression, Aβ Deposition, and Cognitive Impairment in an Alzheimer's Disease Model. J Neurosci. 2017;37(20):5099-5110. https://doi.org/10.1523/jneurosci.2385-16.2017
[22] Narayanan SE, Sekhar N, Rajamma RG, et al. Exploring the Role of Aggregated Proteomes in the Pathogenesis of Alzheimer's Disease. Curr Protein Pept Sci. 2020;21(12):1164-1173. https://doi.org/10.2174/1389203721666200921152246
[23] Wang C, Chen S, Guo H, et al. Forsythoside A Mitigates Alzheimer's-like Pathology by Inhibiting Ferroptosis-mediated Neuroinflammation via Nrf2/GPX4 Axis Activation. Int J Biol Sci. 2022;18(5):2075-2090. https://doi.org/10.7150/ijbs.69714
[24] Aisen PS, Cummings J, Jack CR Jr, et al. On the path to 2025: understanding the Alzheimer's disease continuum. Alzheimers Res Ther. 2017;9(1):60.https://doi.org/10.1186/s13195-017-0283-5

[25] Wei W, Pei H, Ma LN, et al. Comparison of Yizhiqingxin formula extraction methods and their pharmacodynamic differences. Front Neurosci. 2023;17:1097859. https://doi.org/10.3389/fnins.2023.1097859
[26] Gao X, Zhang X, Cui L, et al. Ginsenoside Rb1 Promotes Motor Functional Recovery and Axonal Regeneration in Post-stroke Mice through cAMP/PKA/CREB Signaling Pathway. Brain Res Bull. 2020;154:51-60. https://doi.org/10.1016/j.brainresbull.2019.10.006
[27] Yang SJ, Wang JJ, Cheng P, Chen LX, Hu JM, Zhu GQ. Ginsenoside Rg1 in neurological diseases: From bench to bedside. Acta Pharmacol Sin. 2023;44(5):913-930. https://doi.org/10.1038/s41401-022-01022-1
[28] Ni XC, Wang HF, Cai YY, et al. Ginsenoside Rb1 inhibits astrocyte activation and promotes transfer of astrocytic mitochondria to neurons against ischemic stroke. Redox Biol. 2022;54:102363. https://doi.org/10.1016/j.redox.2022.102363
[29] Sun C, Dong S, Chen W, Li J, Luo E, Ji J. Berberine alleviates Alzheimer's disease by regulating the gut microenvironment, restoring the gut barrier and brain-gut axis balance. Phytomedicine. 2024;129:155624. https://doi.org/10.1016/j.phymed.2024.155624
[30] Singh YP, Rai H, Singh G, et al. A review on ferulic acid and analogs based scaffolds for the management of Alzheimer's disease. Eur J Med Chem. 2021;215:113278. https://doi.org/10.1016/j.ejmech.2021.113278
[31] Wu JJ, Yang Y, Wan Y, et al. New insights into the role and mechanisms of ginsenoside Rg1 in the management of Alzheimer's disease. Biomed Pharmacother. 2022;152:113207. https://doi.org/10.1016/j.biopha.2022.113207
[32] Deng X, Qiu Z, Chen X, et al. Exploring the potential mechanism of ginsenoside Rg1 to regulate ferroptosis in Alzheimer's disease based on network pharmacology. Eur J Pharmacol. 2024;979:176859. https://doi.org/10.1016/j.ejphar.2024.176859
[33] Cheng Y, Shen LH, Zhang JT. Anti-amnestic and anti-aging effects of ginsenoside Rg1 and Rb1 and its mechanism of action. Acta Pharmacol Sin. 2005;26(2):143-149. https://doi.org/10.1111/j.1745-7254.2005.00034.x
[34] Jiang M, Chi J, Qiao Y, et al. Ginsenosides Rg1, Rb1 and rare ginsenosides: Promising candidate agents for Parkinson's disease and Alzheimer's disease and network pharmacology analysis. Pharmacol Res. 2025;212:107578. https://doi.org/10.1016/j.phrs.2025.107578
[35] Cao G, Su P, Zhang S, et al. Ginsenoside Re reduces Aβ production by activating PPARγ to inhibit BACE1 in N2a/APP695 cells. Eur J Pharmacol. 2016;793:101-108. https://doi.org/10.1016/j.ejphar.2016.11.006
[36] Li J, Liu Y, Li W, et al. Metabolic profiling of the effects of ginsenoside Re in an Alzheimer's disease mouse model. Behav Brain Res. 2018;337:160-172. https://doi.org/10.1016/j.bbr.2017.09.027
[37] Xie M, Gu S, Hong Y, et al. Study on the mechanism of Coptis chinensis Franch. And its main active components in treating Alzheimer's disease based on SCFAs using Orbitrap Fusion Lumos Tribrid MS. J Ethnopharmacol. 2023;311:116392. https://doi.org/10.1016/j.jep.2023.116392
[38] Zhiyan C, Min Z, Yida D, et al. Bioinformatic analysis of hippocampal histopathology in Alzheimer's disease and the therapeutic effects of active components of traditional Chinese medicine. Front Pharmacol. 2024;15:1424803. https://doi.org/10.3389/fphar.2024.1424803
[39] Li X, Chen J, Feng W, et al. Berberine ameliorates iron levels and ferroptosis in the brain of 3 × Tg-AD mice. Phytomedicine. 2023;118:154962. https://doi.org/10.1016/j.phymed.2023.154962
[40] Wang C, Zou Q, Pu Y, Cai Z, Tang Y. Berberine Rescues D-Ribose-Induced Alzheimer's Pathology via Promoting Mitophagy. Int J Mol Sci. 2023;24(6):5896. https://doi.org/10.3390/ijms24065896
[41] Zhao Z, Yan J, Huang L, Yang X. Phytochemicals targeting Alzheimer's disease via the AMP-activated protein kinase pathway, effects, and mechanisms of action. Biomed Pharmacother. 2024;173:116373. https://doi.org/10.1016/j.biopha.2024.116373
[42] Gao LJ, Li P, Ma T, et al. Ligustilide alleviates neurotoxicity in SH-SY5Y cells induced by Aβ25-35 via regulating endoplasmic reticulum stress and autophagy. Phytother Res. 2021;35(3):1572-1584. https://doi.org/10.1002/ptr.6925
[43] Xu YJ, Mei Y, Qu ZL, et al. Ligustilide Ameliorates Memory Deficiency in APP/PS1 Transgenic Mice via Restoring Mitochondrial Dysfunction. Biomed Res Int. 2018;2018:4606752. https://doi.org/10.1155/2018/4606752
[44] Kuang X, Zhou HJ, Thorne AH, et al. Neuroprotective Effect of Ligustilide through Induction of α-Secretase Processing of Both APP and Klotho in a Mouse Model of Alzheimer's Disease. Front Aging Neurosci. 2017;9:353. https://doi.org/10.3389/fnagi.2017.00353
[45] Ohashi H, Tsuji M, Oguchi T, et al. Combined Treatment with Curcumin and Ferulic Acid Suppressed the Aβ-Induced Neurotoxicity More than Curcumin and Ferulic Acid Alone. Int J Mol Sci. 2022;23(17):9685. https://doi.org/10.3390/ijms23179685
[46] Zhang L, Guo Q, An R, et al. In vitro ischemic preconditioning mediates the Ca2+/CaN/NFAT pathway to protect against oxygen-glucose deprivation-induced cellular damage and inflammatory responses. Brain Res. 2024;1826:148736. https://doi.org/10.1016/j.brainres.2023.148736
[47] Norris CM. Calcineurin: directing the damage in Alzheimer disease: An Editorial for 'Neuronal calcineurin transcriptional targets parallel changes observed in Alzheimer disease brain' on page 24. J Neurochem. 2018;147(1):8-11. https://doi.org/10.1111/jnc.14475
[48] Song SB, Park JS, Jang SY, et al. Nicotinamide Treatment Facilitates Mitochondrial Fission through Drp1 Activation Mediated by SIRT1-Induced Changes in Cellular Levels of cAMP and Ca2. Cells. 2021;10(3):612. https://doi.org/10.3390/cells10030612
[49] Garbincius JF, Salik O, Cohen HM, et al. TMEM65 regulates and is required for NCLX-dependent mitochondrial calcium

efflux. *Nat Metab*. 2025;7(4):714-729. https://doi.org/10.1038/s42255-025-01250-9